JOURNAL OF MATERIALS SCIENCE **33** (1998) 4769–4773

Simulation of diffusional composite growth using the cellular automaton finite difference (CAFD) method

S. G. R. BROWN
Department of Materials Engineering, University of Wales, Swansea, Singleton Park, Swansea, W. Glamorgan, SA2 8PP, UK

A model is described of directional coupled two-phase composite growth in three dimensions using a combined cellular automaton finite difference (CAFD) approach. The modelling strategy and some preliminary results are presented here for the first time. The model incorporates solute diffusion and a simple cellular automaton growth rule containing a pseudo-curvature algorithm. Despite its limitations, the model is able to simulate some of the structural effects that take place during coupled growth. As a demonstration application the model is applied to eutectic growth in the Pb–Sn system and compared to experimental measurements. The scale of predicted microstructures in the model is close to that measured after directional freezing of Pb–Sn eutectic.

Nomenclature

a	"curvature" constant (K m)
C_{eut}	eutectic composition (wt %)
C_{site}	composition at a given site (wt %)
D	diffusion coefficient ($m^2\ s^{-1}$)
Δx	individual element size (m)
G	preset temperature gradient ($K\ m^{-1}$)
λ	interlamellar spacing (m)
m_α, m_β	liquidus slopes for Pb–Sn phase diagram ($K\ wt\ \%^{-1}$)
n, ϕ	CA rule integer constants (dimensionless)
$n\alpha$, $n\beta$	total number of α and β solid neighbours, respectively, at a given liquid position
P_{site}	phase variable (dimensionless integer flag, range 0–3)
radius (θ)	the radius of a hemisphere of volume θ (m)
T_{eut}	eutectic temperature (K)
T_{site}	temperature at a given site (K)
T_α	calculated liquidus for Pb-rich α-phase solidification at a site (K)
T_β	calculated liquidus for Sn-rich β-phase solidification at a site (K)
x	length (m)

1. Introduction

This paper is concerned with attempting to numerically simulate steady-state, directional, two-phase coupled growth. The model is three-dimensional and combines a finite difference model of solute diffusion with a cellular automaton model that controls the growth of the phases. Since only a limited number of types of coupled growth exist in nature, the solidification of a eutectic alloy (Pb–Sn) has been chosen as a basis for comparison with the model. In this situation a phase transformation of the type, liquid $\rightarrow$ solid α phase + solid β phase occurs, where the solid phases grow in a coupled manner. The progress of this transformation will be affected by a variety of factors. The dominant factors are likely to be growth rate and solute diffusion, although other factors, such as interface curvature and interphase surface energy effects, will also play an important role.

In the case of solidification of a eutectic, the rate at which heat is removed from the system will determine the rate at which the composite solid/liquid interface is able to propagate into the liquid. However, for coupled growth to occur, diffusion in the liquid ahead of the two growing phases must also take place. Controlled experimentation on the unidirectional steady-state growth of eutectics [1–5] has shown how such systems evolve under different conditions. In practice, it is observed that eutectic microstructures are generally finer at higher cooling rates (where there is less time for diffusion to occur) and will coarsen if the cooling rate is reduced.

Initial modelling work in this area consisted of theoretical studies of steady-state eutectic/eutectoid transformations [6–8]. During the last decade, much effort has been spent developing computer-based numerical simulations of microstructural evolution during solidification. Early stochastic growth models of solidification focus on the idea of growing grains within the liquid. Whether these grains are dendritic [9–11] or eutectic [12–14] does not affect the modelling procedure because only the overall grain structure is modelled rather than the microstructural development within grains. Various approaches have been used to model the evolution during freezing of a eutectic structure. Two-dimensional random walk models have been used

to simulate the directional solidification of eutectics in undercooled two-component systems [15, 16]. Three-dimensional (3D) simulations of coupled growth have also been reported using cellular automata techniques [17, 18]. Probably the most sophisticated modelling framework, the phase-field method, has recently been used to model multiphase growth [19, 20] for both eutectics and peritectics. In this paper an extension to a cellular automaton finite difference (CAFD) model, previously used to model alloy dendritic solidification [21, 22], is used to simulate unidirectional composite growth.

2. The model

The 3D model uses a regular cubic lattice of elements where the situation at any given site is defined by three variables, temperature, composition and phase. The temperature and composition values represent real quantities. The phase variable is an integer flag that defines the element as being in one of the following four situations.

- Liquid (no solid neighbours) $P_{\text{site}} = 0$
- Liquid (at least one solid nearest neighbour) $P_{\text{site}} = 1$
- Solid (α phase) $P_{\text{site}} = 2$
- Solid (β phase) $P_{\text{site}} = 3$

As an example, the model is described below in terms of the directional freezing of a Pb–Sn eutectic alloy. It must be noted that no attempt is made to incorporate all those factors known to affect the evolution of eutectic microstructure such as interphase surface energies.

In the following simulations, complete insulation is set as a boundary condition on the top and bottom faces of the grid whereas periodic boundary conditions are used on the other four sides. In addition, a constant temperature gradient, G, is imposed on the grid with the bottom plane of the grid initially set at the lowest temperature. Temperatures increase from the bottom of the grid upwards according to the fixed value of G. Site temperatures are racked down as a function of time according to a preset cooling rate. No account is taken of the latent heat of fusion.

The CA growth model is used to apply simple heuristic rules to all sites on the computational grid. These rules determine whether solidification of a particular phase will occur at a given lattice site considering its current local situation. As in previous dendritic CA models a site solidifies only when the temperature of the site falls below the equilibrium liquidus value (extrapolated) calculated from the composition of the element *and* when there are sufficient nearest neighbour solid sites to satisfy the CA growth rule. (Linear liquidus and solidus lines for the Pb–Sn equilibrium phase diagram are assumed.) A site solidifies with a composition of the extrapolated equilibrium solidus value calculated from the element temperature. Once each site on the grid has been assessed by the CA model, any rejected solute is redistributed from solidifying elements to the surrounding liquid elements. This is done simultaneously for all elements. Solute is then allowed to diffuse between elements using a standard FDM approach. After a fixed number (ϕ) of these growth/diffusion steps, the temperatures of all elements are racked down according to the preset cooling rate. The whole process is then repeated.

The CA algorithm defines the neighbourhood of an element as the 26 elements closest to it. The FDM algorithm only works with the six nearest neighbours to any given element. Solute diffusion is modelled using a straightforward implicit finite difference discretization of the standard Fourier equation

$$\frac{\mathrm{d}C}{\mathrm{d}t} = -D\nabla^2 C \tag{1}$$

For comparison with experimental results a constant diffusion coefficient of $D = 6.7 \times 10^{-10}\,\mathrm{m^2\,s^{-1}}$ was used for solute diffusion in the liquid as proposed in the original work [6]. A condition of no solid state diffusion was assumed.

2.1. Initial conditions

Prior to running the model, an initial distribution of solid sites (pseudonucleation sites) from which further solidification can continue is generated. In this paper, two cases were studied. In the first, the whole of the lowest plane of elements is randomly set to solid. Any given site has an equal probability of being set to either α or β (i.e. $P_{\text{site}} = 2$ or 3). In the second case, a small nucleus consisting of a $3 \times 3 \times 1$-element plate of α and a $3 \times 3 \times 1$-element plate of β, sharing one common 3×1 face, are initially placed at the base of the computational grid. In both cases, all remaining sites are initially set to liquid. The temperature at the base of the grid is initially set to the equilibrium eutectic temperature. The temperatures of elements increase from this position into the liquid according to the preset value of G. This promotes directional solidification from the base of the grid upwards at a constant cooling rate.

2.2. The CA growth rule

In the growth routine, the following simple rules determine the liquidus temperature, based on site composition and the current local neighbourhood, at or below which growth of either solid phase will occur (either T_α or T_β). These calculations are performed in each growth iteration for any elements with $P_{\text{site}} = 1$

$$\text{if } (n\alpha > n) \qquad T_\alpha = T_{\text{eut}} - m_\alpha(C_{\text{eut}} - C_{\text{site}}) - \frac{a}{\text{radius}\,(n\alpha \cdot \Delta x^3)} \tag{2}$$

$$\text{if } (n\beta > n) \qquad T_\beta = T_{\text{eut}} - m_\beta(C_{\text{eut}} - C_{\text{site}}) - \frac{a}{\text{radius}\,(n\beta \cdot \Delta x^3)} \tag{3}$$

Having determined the relevant liquidus temperatures for the site, a decision is made as to whether or not solidification occurs according to the following rule

$$\text{if } (n\alpha > n\beta \text{ and } T_{\text{site}} \leq T_\alpha \text{ and } n\alpha > n) \quad \text{then } P_{\text{site}} = 2 \quad (4)$$

otherwise

$$\text{if } (T_{\text{site}} \leq T_\beta \text{ and } n\beta > n) \quad \text{then } P_{\text{site}} = 3 \quad (5)$$

otherwise

$$\text{if } (T_{\text{site}} \leq T_\alpha \text{ and } n\alpha > n) \quad \text{then } P_{\text{site}} = 2 \quad (6)$$

It can be seen from the CA rule above that the liquidus value, at or below which freezing will occur at a site, is governed by both the composition of the element and a crude "curvature" effect. This curvature effect is applied in two ways. Firstly, sites cannot solidify unless they have at least n solid elements in their local neighbourhood. Secondly, the liquidus values calculated at the site (T_α and T_β) are depressed according to the local 26-element neighbourhood via the "a/radius" term in Equations 2 and 3. The scale of this depression due to "curvature" decreasing as the number of "like" solid neighbours increases.

Thus, the model incorporates growth restriction for both phases arising from either solute rejection/accumulation effects or empirically applied curvature effects. These solute and simple curvature algorithms constitute the very simple basis of the model and are straightforward extensions to CA models used previously to simulate alloy dendritic growth. The position of the solidifying front is monitored by the model as a function of time permitting the rate of movement of the simulated growing interface to be calculated. In common with most CA models, although the rules governing growth of either phase are relatively simple, the resultant evolving structures can be surprisingly complicated.

(The particular values of various constants used in this work are: $\Delta x = 0.2 \times 10^{-6}$ m, $n = 4, \phi = 5$, $a = 10^{-4}$ K m, $T_{\text{eut}} = 456$ K.)

3. Simulation results and observations

Fig. 1 shows the distance travelled by the moving interface as a function of time for three different user-defined cooling rates. In each case, a virtually constant growth rate is observed and the rate of movement of the advancing solid/liquid interface can be calculated. The maximum temperature of the growing interface remains virtually constant between 456.0 and 456.2 K throughout the simulations.

Fig. 2 shows the results of a simulation carried out on a $30 \times 100 \times 75$ grid displayed from two different perspectives. In this simulation the measured rate of movement of the solid/liquid interface was calculated to be 0.784×10^{-6} m s^{-1}. In the left of the picture the bottom face of the grid is visible. On this bottom face the random nucleation of both phases used as the initial condition for the simulation is evident. The two solid phases are shown in white and grey while the liquid phase is not shown. The picture on the right is the same simulation result but orientated so that the growing solid–liquid interface is at the top.

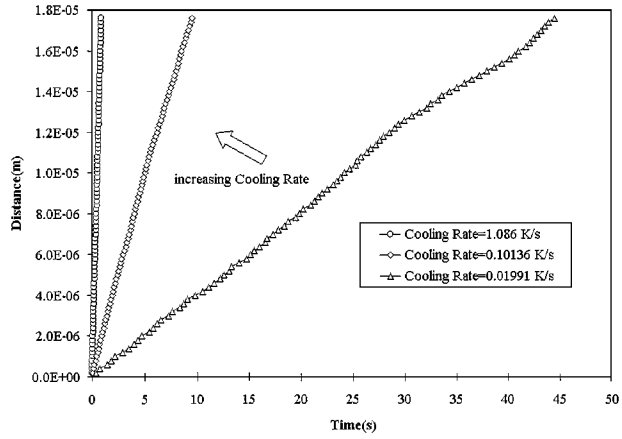

Figure 1 The distance moved by the solid/liquid interface versus time for simulations with different preset cooling rates.

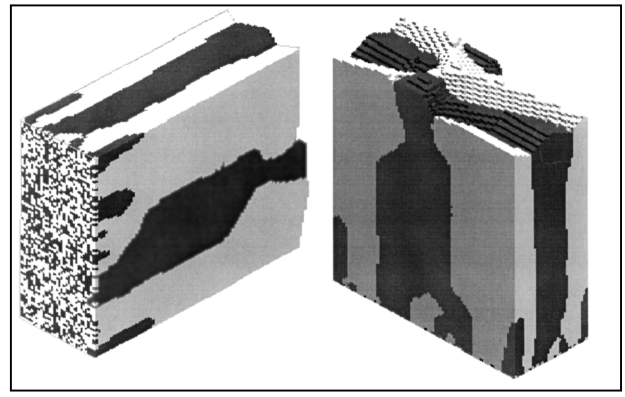

Figure 2 Two views of a simulation carried out on a 225, 000 element grid, with a calculated rate of movement of solid/liquid interface of 0.784×10^{-6} m s^{-1}.

A number of observations can be made. Firstly, a sheet-type structure has formed from the initial random nucleation on the bottom face over a relatively short distance. Secondly, once established, this structure appears to continue growing with only minor morphological changes taking place. In addition, the solid–liquid interface is relatively flat with curvature present for both phases. Because periodic boundary conditions are applied to all side faces it is possible to join up any number of these simulated structures side-by-side to obtain a better overall appreciation of the simulation result. Fig. 3 shows such a picture. In Fig. 3 the left-hand side of the structure has had the top half removed to reveal the lamellar-type structure at a cross-section of the grid.

Fig. 4 shows the predicted structure on exactly the same computational grid but this time using a faster user-defined cooling rate. The rate of movement of the solid–liquid interface was calculated as 0.389×10^{-4} m s^{-1} in the simulation, two orders of magnitude faster than the result in Figs 2 and 3. Comparing this to Fig. 3 it can be seen that the overall microstructure is finer for the faster cooling rate.

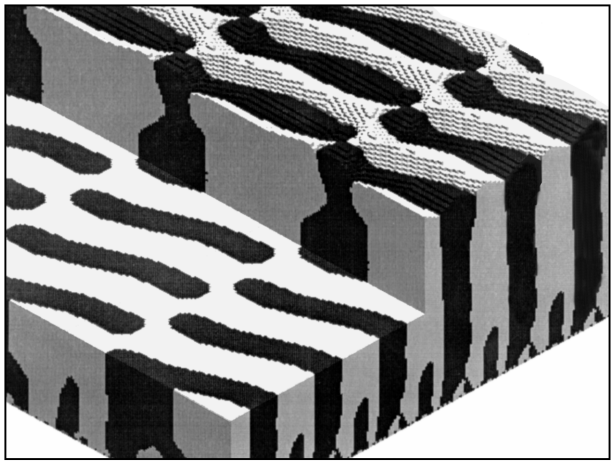

Figure 3 Overall view of predicted microstructure (calculated rate of movement of solid/liquid interface was 0.784×10^{-6} m s^{-1}). The left-hand side of the structure has had top layers of elements stripped away to reveal the morphology below the solid-liquid interface.

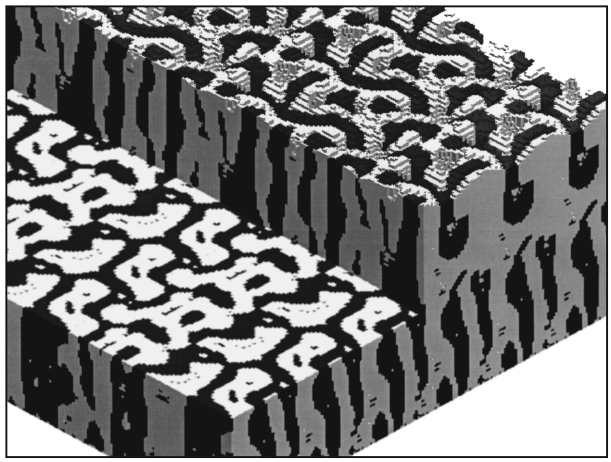

Figure 4 Overall view of predicted microstructure (calculated rate of movement of solid/liquid interface was 0.389×10^{-4} m s^{-1}). The left-hand side of the structure has had top layers of elements stripped away to reveal the morphology below the solid-liquid interface.

The interphase spacings determined from simulated microstructures using a lineal analysis post-processor are compared to values measured by Mollard and Flemings [5] for Pb–Sn alloys in Table I. Experimentally measured values of λ ranged from 1.0–7.55 μm over the whole range studied by Mollard and Flemings. Considering the simplicity of the current CA model the agreement in Table I is considered good.

Fig. 5 shows a composition map for the same results file shown in Fig. 2. The difference in composition between the α, β and liquid phases is clear as is the relative uniformity of composition within each phase.

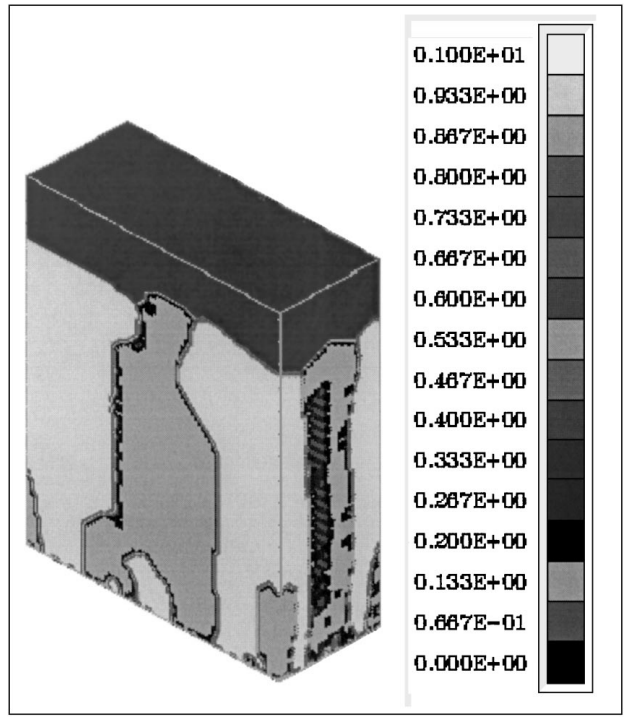

Figure 5 Composition map (wt %) for simulation with calculated rate of movement of solid/liquid interface of 0.784×10^{-6} m s^{-1}.

Similarly, the proportion of α and β phases at the end of the simulations were close to those expected from examination of the Pb–Sn phase diagram.

Although the predicted microstructures do not necessarily resemble actual eutectic structures in the Pb–Sn system, it is noteworthy that the length scales of the simulated structures compare very favourably with measured interlamellar spacings. In addition, it can be seen that the sheet-like structure for the lower growth rate (Figs 2 and 3) appears to have been replaced by a structure consisting of islands of one phase surrounded by the other phase in the higher growth rate simulation (Fig. 4). This alteration in morphology can only be attributed to the length scales over which diffusion of solute can occur at the higher growth rates.

In the simulations described above the growing structure has undergone a coarsening process from an originally fine distribution of random nuclei. In two-dimensional simulations of coupled growth, such coarsening effects are sometimes demonstrated. However, to refine such a growing two-phase structure in a simulation requires either:

- nucleation of one or both phases during growth; or
- a 3D model where refinement can occur by the movement of "lamellar faults" [8].

TABLE I Comparison of published and simulated lamellar spacings

Experimental measured growth rate [5] (m s^{-1})	Calculated growth rate from simulations (m s^{-1})	Measured λ values [5] (μm)	Calculated λ values from simulations (μm)
0.850×10^{-6}	0.784×10^{-6}	6.65, 5.50	3.842
0.300×10^{-4}	0.389×10^{-4}	1.10, 1.10, 1.05	0.974

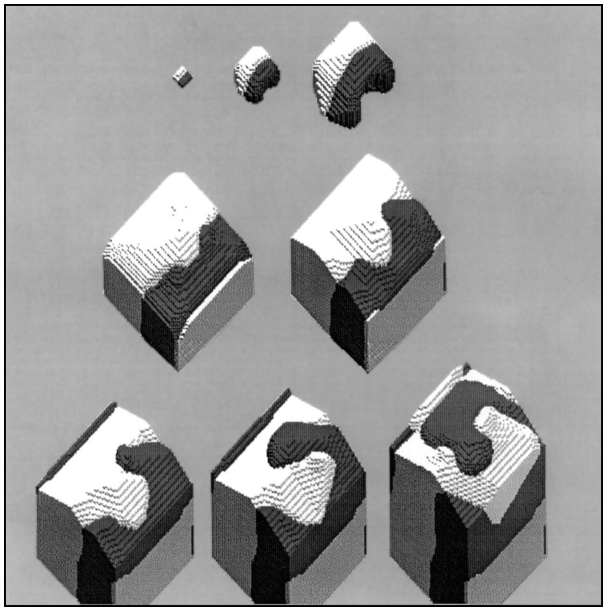

Figure 6 The evolution of simple lamellar faults and simultaneous spacing refinement using a $50 \times 50 \times 100$ grid.

Fig. 6 shows the results of a numerical experiment to determine if the current CA model is capable of refining the microstructural scale without recourse to nucleation. Initially a single nucleus is placed at the base of the grid comprising a $3 \times 3 \times 1$ plate of α-phase adjacent to a $3 \times 3 \times 1$ plate of β-phase. The sequence of the evolving structure can be followed from left-to-right and downwards in Fig. 6.

At first, a virtually flat interface is maintained between the two solid phases. However, after a short time perturbations begin to form and what resemble fingers of either phase begin to spiral around each other. These fingers resemble the lamellar faults described to explain coarsening/refining processes during coupled growth [8]. The movement of these lamellar faults in Fig. 6 is leading to a refinement of the interphase spacing.

4. Conclusions

It has been shown that a simple CA model is capable of simulating some of the phenomena associated with the directional growth of composites. From an initially fine arrangement of random nuclei, the model quickly coarsens to a composite structure that is able to grow in a stable manner. As opposed to coarsening, the ability of the model to refine itself in terms of microstructural length scales has also been demonstrated via a lamellar-fault type of mechanism. Finally, as an example, the model has been applied to the case of directional freezing of Pb–Sn eutectic. Although only solute diffusion and a simple CA growth rule are incorporated into the model good results have been obtained in comparison with some published interlamellar spacing measurements. The model has demonstrated the controlling effect of diffusion on the length scale of the evolving microstructure.

Acknowledgements

The author would like to acknowledge the support of the EPSRC (grant nos. GR/J28575 and GR/K79147) and many helpful discussions with Dr J.A. Spittle.

References

1. J. P. CHILTON and W. C. WINEGARD, *J. Inst. Metals* **89** (1961) 162.
2. J. D. HUNT and J. P. CHILTON, *ibid.* **92** (1963) 21.
3. A. MOORE and R. ELLIOT, in "The solidification of metals" (The Iron and Steel Institute, London, 1968).
4. F. R. MOLLARD and M. C. FLEMINGS, *Trans. Metall. Soc. AIME* **239** (1967) 1526.
5. *Idem., ibid.* **239** (1967) 1534.
6. M. HILLERT, *Jernkontorets Ann.* **141** (1957) 757.
7. W. A. TILLER, in "Liquid metals and solidification" (American Society of Metals, Metals Park, Ohio, 1958).
8. K. A. JACKSON and J. D. HUNT, *Trans. Metall. Soc. AIME* **236** (1966) 1129.
9. S. G. R. BROWN and J. A. SPITTLE, in "Modelling of casting, welding and advanced solidification processes" V, edited by M. Rappaz, M. R. Ozgu and K. W. Mahin (TMS, Warrendale PA, 1990) p. 395.
10. M. RAPPAZ and CH-A. GANDIN, *Acta Metall. Mater.* **41** (1993) 345.
11. CH-A. GANDIN and M. RAPPAZ, *ibid.* **42** (1994) 2233.
12. CH. CHARBON, A. JACOT and M. RAPPAZ, *ibid.* **42** (1994) 3953.
13. M. RAPPAZ, CH. CHARBON and R. SASIKUMAR, *ibid.* **42** (1994) 2365.
14. CH. CHARBON and R. LESAR, *Modelling Simul. Mater. Sci. Eng.* **5** (1997) 53.
15. A. KARMA, *Phys. Rev. Lett.* **59** (1987) 71.
16. J. R. XIAO, J. IWAN, D. ALEXANDER and F. ROSENBERGER, *Phys. Rev. A* **45** (1992) 571.
17. J. A. SPITTLE and S. G. R. BROWN, *Acta Metall. Mater.* **42** (1994) 1811.
18. S. G. R. BROWN and N. B. BRUCE, *J. Mater. Sci.* **30** (1995) 1144.
19. I. STEINBACH, F. PEZOLLA, M. SEESSELBERG, R. PRIELER, G. J. SCHMITZ and J. L. L. REZENDE, *Physica D* **94** (1996) 135.
20. M. SEESSELBERG, J. TIADEN, G. J. SCHMITZ and I. STEINBACH, in Proceedings of the 4th Decennial Int. Conf. On Solidification Processing, edited by J. Beech and H. Jones (SRP Ltd., Exeter, UK, 1997) p. 440.
21. S. G. R. BROWN and J. A. SPITTLE, in "Modelling of casting, welding and advanced solidification processes" VII, edited by M. Cross and J. Campbell (TMS, Warrendale PA 1995) p. 541.
22. J. A. SPITTLE and S. G. R. BROWN, in Proceedings of the 9th International Conference on Numerical Methods in Thermal Problems, edited by R. W. Lewis (Pineridge Press, Swansea 1995) p. 533.

Received 19 January
and accepted 22 July 1998